NEW DEVELOPMENTS IN GRAVITY APPLICATIONS AND INSTRUMENTS

Chris NIND[1]; Tim NIEBAUER[2]

1. Scintrex Ltd, Concord, Ontario, Canada, cnind@scintrexltd.com
2. Micro-g LaCoste Inc, Lafayette, Colorado, USA, tmn@microglacoste.com

INTRODUCTION

Precise measurement of local variations in gravity is a standard earth science exploration tool. Gravity instrumentation has evolved to extend the application of gravity measurements into reservoirs, boreholes and ground shaking. A discussion of each of these applications is presented below (see also Nind, Niebauer et al, 2007)

4D GRAVITY – TRACKING A WATERFLOOD

The world's first 4D surface gravity surveillance of a waterflood was implemented in the Prudhoe Bay oilfield in Alaska in 2002, with surveys being repeated on a yearly basis (Brady et al, 2006). Base ties and gravimeter drift were eliminated by using the Micro-g LaCoste A10 Absolute Gravimeter. Accurate station positioning was achieved using real time kinematic GPS. The original gravity measurements recorded in 2002 and 2003, prior to the start of the waterflood, provide a baseline against which subsequent gravity measurements are compared. The mass introduced by injecting about 40 million tonnes of water annually into the gas cap at about 2,500 metres depth causes a change in gravity at the surface. Gravity measurements taken in March 2006 after two years of waterflood show an increase of over 50 microgals in the immediate vicinity of the injector wells. The location of the waterfront interpreted from the measured data is shown in Figure 1.

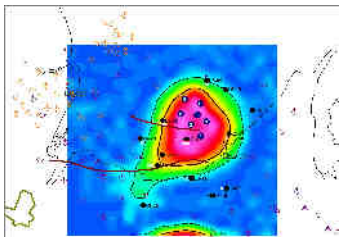

Figure 1: Prudhoe Bay: 2006 –2002 Inversion Mass Model based on 4D Gravity measurements. Water injector wells are shown in blue, monitor wells are shown in black.

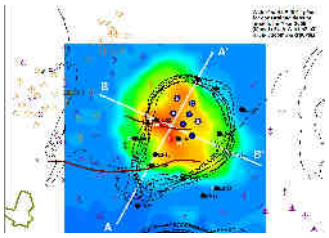

Figure 2: Prudhoe Bay: Reservoir Simulation Mass Compared with 4D Gravity Mass: Leading Edge of Waterfront predicted using the reservoir simulation (colour), and several gravity density models (contour lines).

The density model derived from the 4D Gravity data, supported by the monitor well logs, indicates that more water is flowing to the south and southwest than predicted from the reservoir simulation (Figure 2).

The difference between the apparent location of the mass of injected water based on the reservoir simulation and the gravity models after one and two years of waterflooding along A-A' (Figure 2) is shown on Figure 3. After one year of waterflooding (2005), the 4D Gravity model indicated more water accumulating around the injectors and less water in the fault block northeast of the injectors than predicted by the reservoir simulation. After two years of waterflooding (2006), the 4D Gravity model and the reservoir simulation predict similar volumes of water in the northeast fault block, but the 4D Gravity indicates more water to the southwest than the simulation.

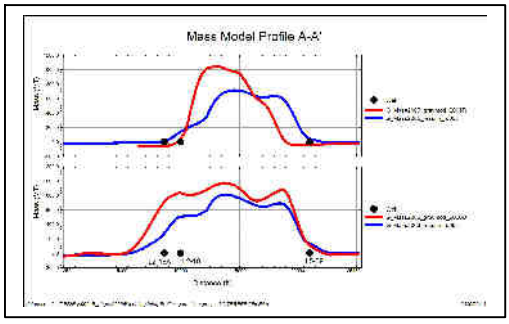

Figure 3: Prudhoe Bay GCWI: SW to NE Profile of 2005 & 06 Reservoir Simulation Mass compared with 4D Gravity Model Mass

The mass inversion based on the 4D Gravity measurements after two years of water injection is overlaid by the reservoir structure map as of March 2006 (Figure 4).

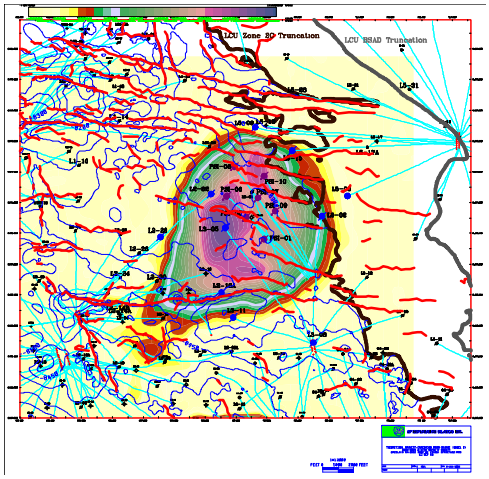

Figure 4: Prudhoe Bay GCWI: Reservoir Structure underlain by 4D Gravity Mass Model as of March 2006.

The 4D Gravity data provide an inexpensive, non-intrusive early warning of developing situations in injection or sequestration projects that can be assessed and, if necessary, remedial actions can be taken.

BOREHOLE GRAVITY – QUANTITATIVE BULK DENSITY MEASUREMENTS

In November and December, 2006, the Pacific Northwest National Laboratories (PNNL) contracted Micro-g LaCoste to collect Borehole Gravity measurements in three boreholes located at the Hanford Waste Treatment Plant in Washington, USA. Gravity measurements were collected every 10 feet in the boreholes, using the L&R Borehole Gravimeter. The purpose of this survey is one which is unique to Borehole Gravity measurements: the determination of the mean bulk density of the rocks traversed by the borehole. LaFehr (1983) and Li & Chouteau (1999) provide the theoretical basis for this method of determining bulk densities. The difference in gravity, corrected for free-air vertical gradient, at two

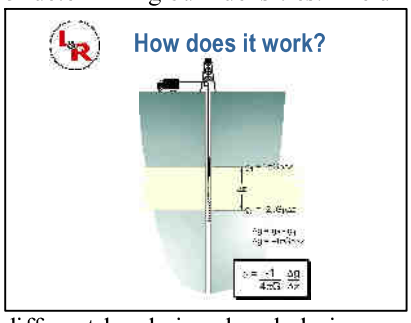

Figure 5: Bulk Density Determination using Borehole Gravity measurements.

different levels in a borehole is proportional to the mean bulk density of the formations between the two levels, to a radius of about 5 times the vertical spacing between the measurements (Herring,

1990). This relationship is illustrated in Figure 5 (downloaded from www.edcon.com). The mean bulk density given by this equation will be an idealized value, as the geology intersected by the borehole will normally not be homogeneous, near-horizontal beds. It does, however, provide a starting point for the interpretation of Borehole Gravity data. (Nind, Seigel et al, 2007)

At Hanford, Borehole Gravity measurement accuracies were better than 5 μGal. Great care was taken to precisely position the gravity sensor at each reading location. The Borehole Gravity data collected at 10 foot intervals provided bulk density measurements of the rocks within about 50 feet of the hole to an accuracy of +/- 0.02 g/cm^3. Figure 6 shows the bulk densities measured by the Borehole Gravity survey compared to the blocked gamma - gamma log over the same 10 foot interval, in one of the three boreholes at Hanford. There is close agreement between the bulk density and the γ-γ density except in areas of washout where the γ-γ measurements are not reliable.

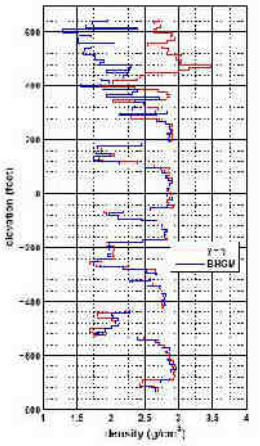

Figure 6: Hanford Waste Treatment Plant, Well C4993: Comparison of Borehole Gravity bulk densities and γ-γ densities

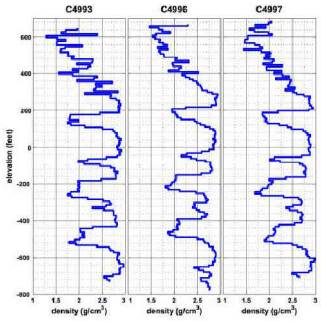

Figure 7: Hanford Waste Treatment Plant: Borehole Gravity Bulk Densities in three boreholes

Bulk density determination of the formations traversed by the borehole can be correlated between boreholes. Figure 7 shows the bulk densities measured in three boreholes separated by about 1,000 feet at the Hanford site. The bulk densities calculated by the Borehole Gravity measurements accurately map the series of high density massive basalt flows in the sedimentary package. Bulk density measurements of formations extending laterally to greater distances from the borehole can be achieved by using wider station intervals.

The accurate determination of bulk densities of the formations traversed by the borehole is unique to Borehole Gravity measurements. Applications include monitoring the advance of waterfronts in high porosity thief zones within petroleum reservoirs, grade control in iron ore mines, rock integrity and void detection for foundations of bridges and large structures and monitoring the integrity of reservoirs during sequestration programs.

GROUND SHAKING – ACCURATE DETECTION OF LONG PERIOD OSCILLATION

Long period ground movements are measured with relative gravity meters capable of detecting small changes of the Earth's gravity with a precision of a few microgals over one second. Gravity meters designed to measure earth tides saturate with the high wave amplitudes and high frequency signals experienced during the initial arrivals after a large earthquake (Niebauer et al, 2007). Seismometers are commonly used to measure the high frequency (0.1-10Hz) and high amplitude signals associated with earthquakes, but their response to frequencies lower than 0.01 Hz is rapidly attenuated. The final report from the 2004 Incorporated Research Institutions for Seismology (IRIS) workshop on broadband seismometers summarized the situation:

"For nearly a quarter of a century, the development of seismic sensors with low noise and high resolution in the normal mode frequency band (0.3-7 milliHertz) has languished. The seismometer of choice for this field of seismology is now over 20 years old, and is no longer being manufactured. Newer sensors, albeit more portable and physically robust, more energy efficient, and less expensive, are less capable of recording Earth motions in this frequency band." (IRIS report, 2004)

Vertical ground motion in the normal mode frequency band are recorded using a superconducting gravity meter, but the high cost and complex operation of this type of gravimeter has limited its use.
In 2006, Micro-g LaCoste introduced a new type of metal spring sensor gravity meter (the "gPhone") that has a large dynamic range to avoid saturation from the high amplitude signals during an earthquake while still having enough sensitivity to record the continuous background seismic and earth tide activity. The earthquake in the Kuril Islands, Japan, on January 13, 2007, provided an opportunity to compare the gPhone with the Streckeisen STS-2 long period seismometer and the GWR SG superconducting gravity meter at a location in Walferdange, Luxembourg.
Figure 8 is a location map with key statistics of the Kuril Islands earthquake, provided by the Earthquake Research Institute at the University of Tokyo (Yamanaka, 2007)

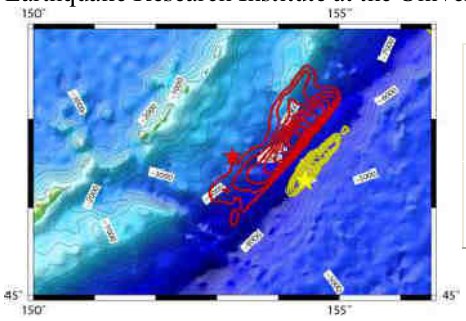

DATE(UT)	07/01/13 04:23
Lon,Lat,Dep (USGS)	46.288 N 154.448 E 10km
M(USGS)	8.2
Depth	7 km

Figure 8: Earthquake of 8.2 magnitude, 07/01/13 04:23(UT) Kuril Islands, Japan

The P-wave arrived in Luxembourg about 12 minutes after the earthquake, followed by the S-wave (13 minutes later) and the surface wave (40 minutes after the earthquake). The event was recorded on the broadband seismometer and the two gravity meters.
Figure 9 compares the records of the earthquake on the SG superconducting gravity and the gPhone. The SG meter saturates during the earthquake.

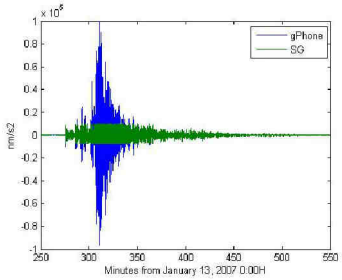

Figure 9: Vertical ground accelerations recorded in Luxembourg after the Kuril Islands earthquake on an SG gravity meter (green) and a gPhone (blue)

The gPhone did not saturate during the earthquake and the sensitivity of the meter matches the SG meter at other times. Figure 10 compares vertical ground accelerations recorded by the GPhone and SG gravity meters one hour before the earthquake. The vertical ground accelerations during this period of normal activity are three orders of magnitude smaller than the accelerations recorded on the gPhone during the earthquake. The records of the two gravity meters closely match during periods of normal activity.

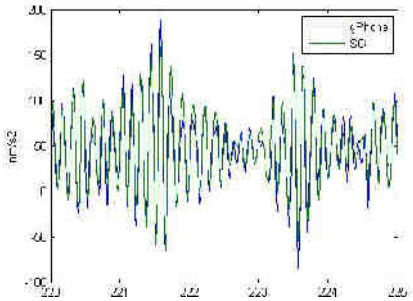

Figure 10: Vertical ground accelerations recorded in Luxembourg, during a period of normal activity, on an SG gravity meter (green) and a gPhone (blue)

The gPhone accelerations were integrated to yield vertical ground velocities for comparison with the STS-2 seismometer data. Figure 11 shows the vertical ground velocity response recorded by the STS-2 (bottom) and the calculated gPhone velocities (top)

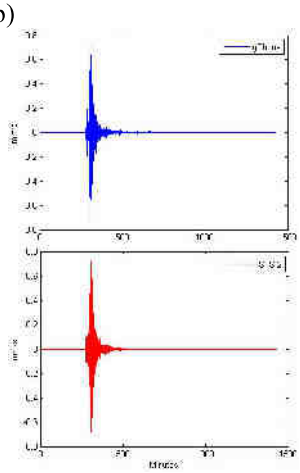

Figure 11: Vertical ground velocities recorded in Luxembourg after the Kuril Island earthquake on an STS-2 broadband seismometer (red) and a gPhone after integration (blue)

The only noticeable difference between the two records is the reoccurrence of disturbances on the gPhone trace after the earthquake. Figures 12 and 13 compare the vertical ground velocities recorded by the STS-2 and the gPhone over five minute periods during the earthquake (Figure 12) and several hours after the earthquake (Figure 13).

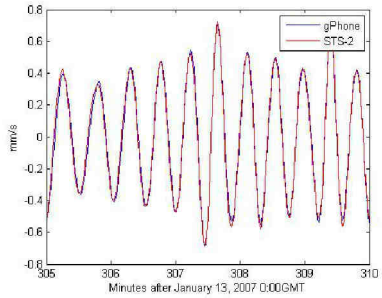

Figure 12: Vertical ground velocities during the S-wave arrivals after the Kuril Islands earthquake.

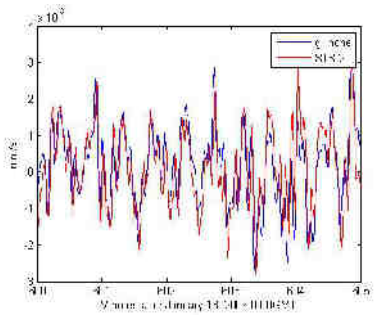

Figure 13: Vertical ground velocities recorded five hours after the Kuril Islands earthquake.

The match between the STS-2 data and the gPhone integrated data is very close, even during periods of normal activity when the vertical ground velocities are three orders of magnitude smaller than those recorded during the earthquake.

In order to explain the repeated occurrence of ground disturbances on the gPhone record (Figure 11), the gPhone data were integrated a second time to yield apparent ground disturbances. The vertical ground disturbances recorded by the gPhone during the earthquake are shown in Figure 14.

Rayleigh wave arrival times from both directions can be calculated using approximate velocities in either direction from Japan to Luxembourg. The Rayleigh wave arrival times observed in the gPhone data closely match the model-predicted times, Figure 15.

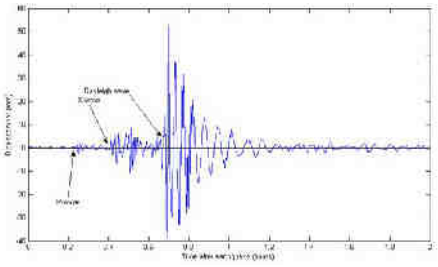

Figure 14: Apparent vertical ground disturbances recorded in Luxembourg, during the Kuril Island earthquake, on a gPhone after double integration.

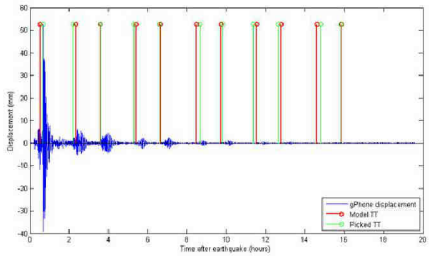

Figure 15: Rayleigh wave arrival times in Luxembourg, after the Kuril Islands earthquake. The arrival times observed in the gPhone data (green) match the model-predicted times (red).

The gPhone recorded 11 Rayleigh wave arrivals (6 forward arc, 5 reverse arc). By comparison, the STS-2 seismometer recorded two arrivals.
The gPhone's sensitivity and dynamic range suggests that further analysis of ground shaking recorded by this instrument, both during an earthquake and during normal periods, should be done. The gPhone is portable and easy to use, allowing it to be deployed optimally.

CONCLUSIONS

New gravity instrumentation has been developed for new applications of the gravity method. This paper briefly summarizes four such applications: 4D Gravity Reservoir Monitoring, Borehole Gravity, and Long Period Ground Motions. Gravity interpretation tools are readily available and well understood. Waterflooding and sequestration projects of sufficient size can be monitored with 4D absolute gravity surveys. Bulk densities of underground formations can be accurately obtained using precise borehole gravity measurements. Long period ground motions can be measured using portable, affordable gravity meters designed for this purpose. Other new applications of the gravity method have been omitted from this paper due to space limitations, but it is hoped that the reader will, from these four examples, conclude that the utility of the gravity method extends far beyond the standard "gravity survey" commonly employed in geophysical exploration.

REFERENCES

Brady, J.L., Hare, J.L., Ferguson, J.F., Seibert, J.E., Klopping, F.J., Chen, T., and Niebauer, T.M.2006. Result of the World's First 4D Microgravity Surveillance of a Waterflood – Prudhoe Bay, Alaska, SPE 101762, 2006 SPE Annual Technical Conference and Exhibition, San Antonio, TX.

Ingate, S. and Berger, J., 2004. Incorporated Research Institutions for Seismology: Prospects for Low-Frequency Seismometry, A Report if the IRIS Broadband Seismometer Workshop, Granlibakken, CA.

Herring, A.T., 1990. Introduction to Borehole Gravity: www.edcon.com, Edcon, Inc, Denver, CO.

LaFehr, T.R., 1983. Rock density from Borehole Gravity Surveys: Geophysics, 48 (3), p. 341-356.

Li, X., and Chouteau, M., 1999. On Density Derived from Borehole Gravity: Log Analyst 40 (1), p. 33-38.

Nind, C., Niebauer, T., MacQueen, J., Van Westrum, D., Klopping, F., Aliod, D., Mann, E., Francis, O., 2007. New Developments in Gravity Applications and Instruments: International Petroleum and Natural Gas Congress & Exhibition of Turkey (IPETGAS 07), proceedings # 1006.

Nind, C., Seigel, H.O., Chouteau, M., Giroux, B., 2007. Development of a Borehole Gravimeter for Mining Applications: EAGE First Break, 25, July 2007, p. 71-77.

Yamanaka, Y., 2007. 07/01/13 04:23 (UT) Kuril Islands, EIC Seismological Note No. 184, www.eri.u-tokyo.ac.jp/sanchu/Seismo_Note/2007/EIC184e.html, ERI, University of Tokyo.